ELSEVIER

Biophysical Chemistry 63 (1996) 1–16

Biophysical Chemistry

Characterization of Eu(III) binding to a series of calmodulin binding site mutants using laser-induced Eu(III) luminescence spectroscopy [1]

JoAnne Bruno [a], William De W. Horrocks Jr. [a,*], Kathy Beckingham [b]

[a] *Department of Chemistry, The Pennsylvania State University 152 Davey Laboratory, University Park, PA 16802, USA*
[b] *Department of Biochemistry and Cell Biology, Rice University Houston, Houston, TX 77005, USA*

Received 25 September 1995; accepted 8 March 1996

Abstract

Laser-induced luminescence techniques were used in a rigorous evaluation of the Eu^{3+}-binding behavior of a recombinant (*Drosophila melanogaster*) calmodulin and a series of calmodulin binding site mutants in which the bidentate glutamic acid residue in position 12 of each metal ion binding loop is systematically replaced with lysine. For the range of Ca^{2+} concentrations at which calmodulin functions (10^{-5}–10^{-6} M), Ca^{2+} binding is effectively eliminated at the mutated site; however, the luminescence studies show that the Eu^{3+} ion binds to the modified site with reduced affinity. The mutations do not significantly change the intermetal ion distances from their wild type values. These were determined by $Eu^{3+} \rightarrow Nd^{3+}$ Förster-type non-radiative energy transfer experiments. Consistent with the results of Ca^{2+}-binding studies, mutation of sites II and IV in the N- and C-terminal domains, respectively, produces a larger alteration in the Eu^{3+}-luminescence and Eu^{3+}-binding behavior than does mutation of sites I and III. Modification of either of the sites in the C-terminus (III or IV, numbered from the amino terminus) causes two additional H_2O molecules (four H_2O molecules total) to bind to the Eu^{3+} ion in order to compensate for the loss of the bidentate glutamic acid residue. Consequently, the partner site in the domain loses an H_2O molecule, thereby coordinating another ligand from the protein. Mutation of either of the high-affinity Ln^{3+}-binding sites (I or II) has global effects on the Eu^{3+}-binding behavior of the protein molecule.

Keywords: Lanthanide ion probes; Calcium-binding protein; Metal ion binding constants; Metal-coordinated water molecules; Förster-type nonradiative energy transfer; Distance measurements

Abbreviations: BCaM, bovine testes calmodulin; CaM, calmodulin; DmCaM, *Drosophila melanogaster* calmodulin; edta, ethylenediaminetetraacetic acid; equiv, equivalents; fwhm, full width at half-maximum; K_d, dissociation constant; Ln^{3+}, trivalent lanthanide ions; OCaM octopus calmodulin

* Corresponding author.

[1] This work was supported by the National Institutes of Health (Grant GM23599 to W.D.H. and Grant GM49155 to K.B.), the Texas Higher Education Board (Grant 003604-042 to K.B.), and the Welch Foundation (Grant C-1119 to K.B.).

PII S0301-4622(96)02179-5

1. Introduction

Sequence homology among Ca^{2+}-binding proteins in the calmodulin (CaM) superfamily is most pronounced in the 'EF-hand' Ca^{2+}-binding regions. For many of these proteins, three coordinating residues in the 12-residue binding loop are invariant: an aspartic acid residue in position 1, a glycine in position 6, and a glutamic acid in position 12 [1,2]. The glutamic acid residue in position 12 appears to be responsible for 'locking' the Ca^{2+} ion in place, since both of the carboxylate oxygen atoms are bound [3,4], in contrast to the other carboxylate residues (Asp, Glu) in the loop which bind in a monodentate fashion.

Maune and co-workers [5,6] have generated a series of mutants of the *Drosophila melanogaster* calmodulin isotype (subject of the present study) in which the glutamic acid residue at position 12 in each binding loop is replaced systematically with a glutamine or lysine. The glutamine residue was chosen as a conservative change with the potential for Ca^{2+} ligation through the amide oxygen atom, while the lysine substitution was viewed as a more radical alteration that would abolish Ca^{2+} binding owing to spatial considerations, charge reversal, and the lack of an oxygen-bearing group. Their results indicate that Ca^{2+}-binding at the mutated site is severely impaired (K_ds in the millimolar range) for both of the chosen substitutions, while the Ca^{2+}-binding affinity of the nonmutated site in the same domain is also reduced.

Laser-induced luminescence studies of Eu^{3+} substituted into the EF-hand sites of Ca^{2+}-binding proteins have provided insight into the metal ion binding behavior and structure of this class of proteins. The spectroscopically silent Ca^{2+} ion may be replaced by the Eu^{3+} ion owing to the nearly identical ionic radii of these ions (7-coordinate Ca^{2+} 1.20 Å; 8-coordinate Eu^{3+} 1.21 Å). The additional positive charge on the lanthanide ions (Ln^{3+}) causes them to bind 2–5 orders of magnitude more tightly with a given set of ligands than does Ca^{2+}. In addition, Ln^{3+} ions generally achieve a coordination number greater by one, often by ligating an additional water molecule. A detailed comparison of Ln^{3+} and Ca^{2+} binding in biological systems [7], and a comprehensive discussion of Ln^{3+} luminescence [8] are available.

Although studies have shown an opposite binding order for the native Ca^{2+} ion and Ln^{3+} ion probes (the latter bind first to sites I and II; [9–11]), excitation spectroscopy of the $^7F_0 \rightarrow {}^5D_0$ transition of the Eu^{3+} ion bound to either a vertebrate (bovine testes [12,13]) or an invertebrate (octopus [14]) CaM has provided a wealth of information regarding the metal binding characteristics of this important protein. The present study characterizes the Eu^{3+}-binding behavior of wild type DmCaM and the lysine series of binding site mutants using laser-induced Eu^{3+} luminescence techniques, and attempts to identify the metal binding and structural consequences of modifying the metal-binding loops in an effort to provide further understanding of the metal ion binding mechanisms intrinsic to calmodulin. These studies are important to the assessment of the ability of the Eu^{3+} luminescence probe technique to report on modifications made at Ca^{2+} ion binding sites, and of the applicability of the results to consequences for Ca^{2+} binding.

2. Materials and methods

2.1. Preparation of protein samples

Wild type DmCaM and the mutant proteins were prepared as described previously [5]. The nomenclature system used by Beckingham [4] to identify the mutant proteins is employed here; mutation of the glutamic acid in binding loop I (E31K) is denoted B1K, loop II (E67K) B2K, loop III (E104K) B3K, and loop IV (E140K) B4K. Edta removal and buffer exchange were conducted as outlined by Bruno et al. [14]. Polymetal Sponge B (Molecular Probes, Inc.) was used to remove Ca^{2+} from the protein samples and buffers according to a previously described procedure [16]. Protein concentrations were determined using the reported molar absorptivities [5], and the BCA protein assay (Pierce) with both bovine serum albumin and BCaM as standards.

2.2. Eu^{3+} luminescence titrations

$EuCl_3 \cdot 6H_2O$ and D_2O (99.8%) were obtained from Aldrich Chemical Co. All metal ion solutions were standardized by a chelometric technique [15]. All protein samples (10–15 μM) were buffered in

50 mM Hepes at pH or pD 7.0 and made 500 mM in KCl in order to avoid nonspecific Ln^{3+} binding and the resulting precipitation that occurs at lower salt concentrations. A Nd:YAG (Continuum Series YG581-C) pumped tunable dye laser (Model TD150) pulsed at 10 Hz (60–90 mJ/pulse) was used to obtain the data; the details of this system are presented elsewhere [17,18]. The $^7F_0 \rightarrow {}^5D_0$ transition of the Eu^{3+} ion was excited with laser light at 578–581 nm (pulse width 7 ns; resolution 0.01 nm), and the $^5D_0 \rightarrow {}^7F_2$ emission was monitored at 612 nm for all experiments.

Excitation spectral bands were decomposed into their component peaks using the commercially available program PeakFit (Jandel Scientific), which employs an algorithm based on the nonlinear least-squares regression method developed by Marquardt [19], and a Lorentzian–Gaussian lineshape function, which has been shown to yield the best fits for Eu^{3+} luminescence data [20]. The quality of a given fit to the data was evaluated by plots of a weighted fit of the data (see Fig. 1) and minimization of χ^2. Knowledge of the system under study was also applied in deciding whether to accept a fit, because more parameters (i.e. component peaks) generally yields smaller χ^2 values; however, all of the derived parameters may not be valid for the system. Component peak parameters and excited-state lifetime values (see below) that were resolved at low metal-to-protein ratios where the Eu^{3+} ion luminescence is less complex (vide infra) were held constant at higher metal-to-protein ratios in order to simplify the analysis. In evaluating the quality of a fit to the data in which parameters were fixed, the χ^2 value obtained was compared to a fit in which all of the parameters were free floating [20,21].

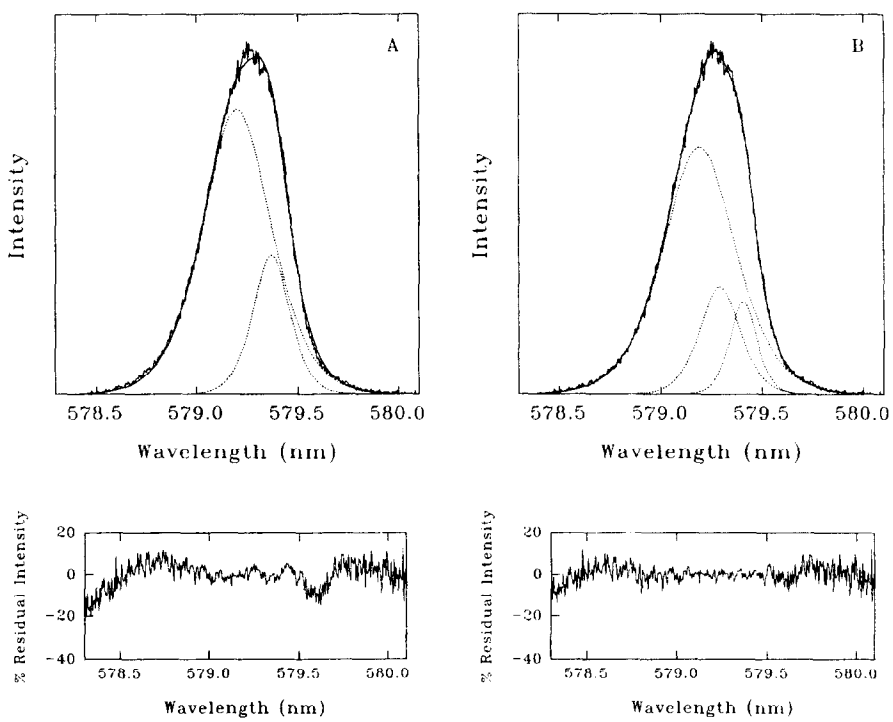

Fig. 1. Curve-resolved $^7F_0 \rightarrow {}^5D_0$ excitation spectra of 1 equiv of Eu^{3+} bound to B4K (13 μM) fit with (A) two and (B) three Lorentzian–Gaussian peaks. The parameters of the fit are: (A) $\lambda_1 = 579.20$ nm, $\sigma_1 = 0.39$ nm; $\lambda_2 = 579.37$ nm, $\sigma_2 = 0.22$ nm; and (B) $\lambda_1 = 579.20$ nm, $\sigma_1 = 0.42$ nm; $\lambda_2 = 579.29$ nm, $\sigma_2 = 0.23$ nm; $\lambda_3 = 579.41$ nm, $\sigma_3 = 0.15$ nm; where λ and σ are the wavelength of the peak maximum and fwhm, respectively. Plots of the percent residual intensity (calculated vs observed) are shown for comparison of fit quality.

Data collection for steady state and time-resolved experiments has been described previously [14,16]; all data were corrected for laser power fluctuations. The multiexponential decays were analyzed into a sum of component functions using PeakFit and the quality of the fit was evaluated as described above.

2.3. Dissociation constant measurements

Binding isotherms were obtained by plotting either the total luminescence intensity obtained at a given excitation wavelength (steady state experiments), the individual amplitudes (intensity at time $t = 0$; time-resolved experiments), or component peak intensities resolved from excitation spectra as a function of Eu^{3+} ion concentration. Theoretical fits of the titration data were calculated using the program EQUIL [22], which is based on a general thermodynamic model of chemical equilibria. Where the quality of the data permitted, binding curves obtained for each type of experiment (spectral peak resolution, and steady state and time-resolved at multiple excitation wavelengths) were analyzed simultaneously using the same set of equilibrium equations to calculate the dissociation constants. Minimization of χ^2 and visual inspection of the agreement between the theoretical fit and the data (titration curve) provided the basis for accepting or rejecting a particular binding model. For cases where simultaneous fitting of multiple data sets was conducted, the goodness of the fit was also evaluated by the agreement between χ^2 for the composite fit and the sum of the χ^2 values for the individual data sets. It should be noted here that the dissociation constants derived by this method for Eu^{3+} binding are site or intrinsic constants, in contrast to the Ca^{2+}-binding experiments [5], which measured macroscopic dissociation constants.

3. Results

3.1. $^7F_0 \rightarrow {}^5D_0$ excitation spectroscopy of wild type and mutant DmCaM

The $^7F_0 \rightarrow {}^5D_0$ excitation spectrum of the Eu^{3+} ion bound to wild type DmCaM is characterized by a relatively broad band (fwhm = 0.44 nm) whose intensity increases as Eu^{3+} is added to the apo-protein,

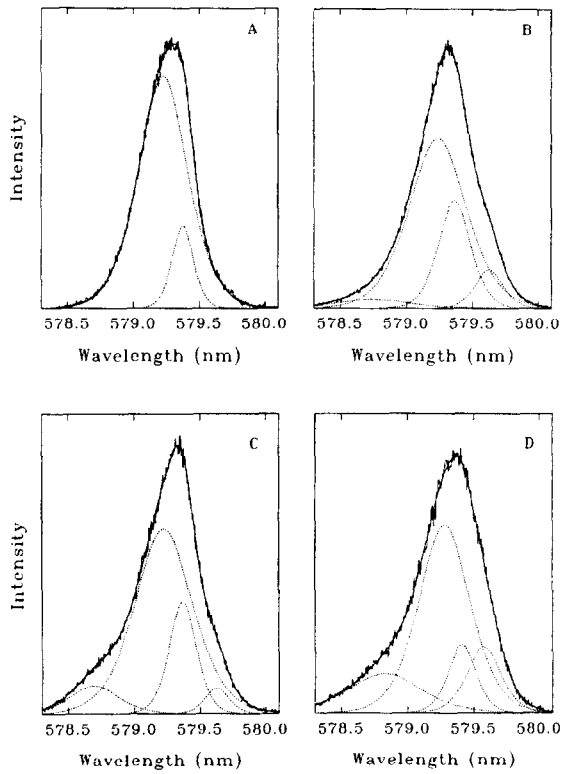

Fig. 2. Curve-resolved $^7F_0 \rightarrow {}^5D_0$ excitation spectra of: (A) 1 equiv; (B) 4 equiv of Eu^{3+} bound to wild type DmCaM (15 μM); (C) 4 equiv of Eu^{3+} bound to B3K (13 μM); (D) 4 equiv of Eu^{3+} bound to B4K (13 μM). The parameters of the fit are: (A) $\lambda_1 = 579.23$ nm, $\sigma_1 = 0.43$ nm; $\lambda_2 = 579.38$ nm, $\sigma_2 = 0.19$ nm; and (B) $\lambda_1 = 578.75$ nm, $\sigma_1 = 0.66$ nm; $\lambda_2 = 579.25$ nm, $\sigma_2 = 0.50$ nm; $\lambda_3 = 579.38$ nm, $\sigma_3 = 0.28$ nm; $\lambda_4 = 579.61$ nm, $\sigma_4 = 0.26$ nm; (C) $\lambda_1 = 578.74$ nm, $\sigma_1 = 0.52$ nm; $\lambda_2 = 579.25$ nm, $\sigma_2 = 0.48$ nm; $\lambda_3 = 579.38$ nm, $\sigma_3 = 0.22$ nm; $\lambda_4 = 579.63$ nm, $\sigma_4 = 0.21$ nm; (D) $\lambda_1 = 578.83$ nm, $\sigma_1 = 0.65$ nm; $\lambda_2 = 579.26$ nm, $\sigma_2 = 0.48$ nm; $\lambda_3 = 579.40$ nm, $\sigma_3 = 0.25$ nm; $\lambda_4 = 579.57$ nm, $\sigma_4 = 0.31$ nm; where λ and σ are the wavelength of the peak maximum and fwhm, respectively.

but whose peak shape and excitation maximum vary little throughout a titration (Fig. 2(A), 2(B)). The position of the peak maximum shifts from 579.26 to 579.32 nm, and a slight shoulder is observed at ~ 579.6 nm after the addition of 2 equiv of Eu^{3+} (Fig. 2(B)). The excitation band was decomposed into its component peaks as outlined in the Materials and Methods section. Because neither the $^7F_0$ (ground) nor the $^5D_0$ (excited) state is split by the ligand field, in principle each distinct Eu^{3+} ion environment is represented by a single peak. Prior to the addition of

Table 1
Summary of the Lorentzian–Gaussian peak parameters determined for the curve-resolved $^7F_0 \rightarrow {}^5D_0$ excitation spectra of Eu^{3+} bound to *Drosophila melanogaster* calmodulin and the lysine series of mutants

Mutant	Equiv Eu^{3+}	λ, nm	fwhm, nm
Wild type	0–2	579.23	0.44
		579.38	0.19
	2–6	579.25	0.50
		579.38	0.28
		579.61	0.26
B3K	0–2	579.24	0.45
		579.38	0.20
	2–6	579.24	0.48
		579.38	0.22
		579.63	0.21
B4K	0–2	579.20	0.39
		579.37	0.22
	0–2	579.20	0.42
	alternate	579.29	0.23
		579.41	0.15
	2–6	579.26	0.48
		579.40	0.25
		579.57	0.31
B1K	0–6	579.1	0.6
		579.2	0.7
		579.35	0.39
		579.65	0.29
		579.61	0.23
B2K	0–1.5	579.07	0.53
		579.42	0.37
		579.60	0.33
	1.5–6	579.17	0.64
		579.38	0.37
		579.62	0.28

2 equiv of Eu^{3+}, a good fit is achieved with two Lorentzian–Gaussian functions ($\lambda_1 = 579.23$ nm, $\lambda_2 = 579.38$ nm; Fig. 2(A) and Table 1); these two peaks are attributed to Eu^{3+} binding to sites I and II (high-affinity Ln^{3+} sites). At higher metal ion concentrations where all of the binding sites are populated by Eu^{3+}, only three of the four expected peaks are resolved from the excitation spectrum, owing to a near coincidence in band wavelengths. The three peaks identified in Fig. 2(B) represent the best fit of the data as judged by plots of the weighted residuals and minimization of χ^2; the fourth peak shown in the curve-resolved spectrum ($\lambda = 578.75$ nm) indicates the presence of the free Eu^{3+}_{aq} ion. Equivalent spectral features are observed during a titration of BCaM [12,13] and OCaM [14].

The parameters (peak position, fwhm) that describe the individual peaks in the $^7F_0 \rightarrow {}^5D_0$ excitation spectrum recorded for up to 2 equiv of Eu^{3+} added to B3K are virtually identical to those obtained for the unmodified protein (Table 1). At higher Eu^{3+} concentrations (2–3 equiv), the curve-resolved $^7F_0 \rightarrow {}^5D_0$ excitation spectra observed for B3K are also similar to those seen for native DmCaM, with the exception that the shoulder at ~ 579.6 nm is less pronounced, and a fourth peak in the region of the Eu^{3+}_{aq} ion arises before 4 equiv of Eu^{3+} have been added (Fig. 2(C)).

The overall shape of the excitation spectra recorded for less than 2 equiv of Eu^{3+} added to B4K also resembles that observed for native DmCaM; however, the excitation band is best described by three Lorentzian–Gaussian peaks (compare Fig. 1(A) and 1(B)). The χ^2 value for the two-peak description is reduced ~ 50% by incorporating a third band into the analysis, and consequently, the weighted plots of the residuals are improved markedly (Fig. 1). Additional Eu^{3+} luminescence data (e.g. excited-state τ values, Eu^{3+} binding isotherms — see below) do not indicate population of three binding sites; therefore, it appears that mutation of site IV alters one of the Eu^{3+} ion environments in the N-terminus such that a single site gives rise to two peaks in the excitation spectrum. This phenomenon has been observed previously for Eu^{3+} bound to the Ca^{2+}-binding sites of parvalbumin [23,24] and calcineurin B [25]. Only one of the bands resolved in the three-peak fit (579.20 nm) resembles a peak observed in the excitation spectrum of the wild type protein (Table 1).

At higher metal-to-protein ratios, only the 579.40 nm peak observed in the excitation spectra of B4K prior to the addition of 2 equiv of Eu^{3+} is present; the 579.23 nm peak is obscured by the most intense band which is red-shifted (579.20 → 579.26 nm) relative to the species resolved at lower Eu^{3+} concentrations (Fig. 2(D)). After the addition of ~ 3 equiv of Eu^{3+}, a fourth peak becomes apparent in the region of the spectrum where free Eu^{3+}_{aq} is observed (578.3–579.1 nm).

The $^7F_0 \rightarrow {}^5D_0$ excitation spectrum of the Eu^{3+} ion bound to B1K or B2K indicates that the Eu^{3+}

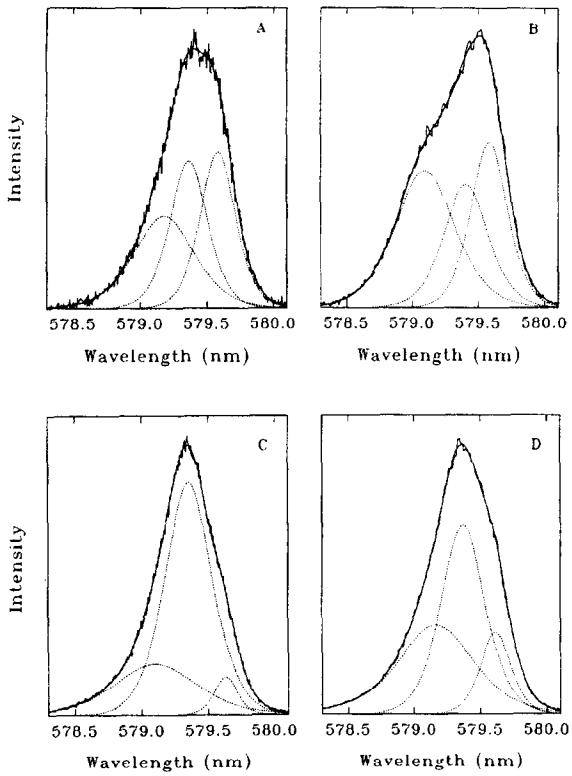

Fig. 3. Curve-resolved $^7F_0 \rightarrow {}^5D_0$ excitation spectra of (A) 0.25 equiv and (C) 4.0 equiv of Eu^{3+} bound to B1K (15 μM); (B) 0.40 equiv and (D) 4.0 equiv of Eu^{3+} bound to B2K (μM). The parameters of the fit are: (A) $\lambda_1 = 579.18$ nm, $\sigma_1 = 0.53$ nm; $\lambda_2 = 579.36$ nm, $\sigma_2 = 0.33$ nm; $\lambda_3 = 579.58$ nm, $\sigma_3 = 0.31$; (B) $\lambda_1 = 579.09$ nm, $\sigma_1 = 0.53$ nm; $\lambda_2 = 579.42$ nm, $\sigma_2 = 0.39$ nm; $\lambda_3 - 579.58$ nm, $\sigma_3 = 0.32$; (C) $\lambda_1 = 579.10$ nm, $\sigma_1 = 0.73$ nm; $\lambda_2 = 579.35$ nm, $\sigma_2 = 0.42$ nm; $\lambda_3 = 579.63$ nm, $\sigma_3 = 0.20$ nm; and (D) $\lambda_1 = 579.17$ nm, $\sigma_1 = 0.64$ nm; $\lambda_2 = 579.38$ nm, $\sigma_2 = 0.37$ nm; $\lambda_3 = 579.62$ nm, $\sigma_3 = 0.28$ nm; where λ and σ are the wavelength of the peak maximum and fwhm, respectively.

ion environments are altered dramatically by the mutation of sites I and II. As shown in Fig. 3(A) and 3(B), both mutants display an excitation band that is broader than that observed for the wild type protein at the titration outset (fwhm = 0.46 nm B1K, 0.70 nm B2K vs 0.44 nm DmCaM), and consists of three Lorentzian–Gaussian peaks with excitation maxima at ~ 579.1, 579.4, and 579.6 nm and peak widths (fwhm) of ~ 0.6, 0.4, and 0.3 nm (Table 1). As the sites of either B1K or B2K continue to fill with Eu^{3+}, the number of component peaks in the excitation band does not change; the parameters for these peaks are summarized in Table 1. At higher Eu^{3+} concentrations the overall shape of the excitation band for both B1K and B2K approaches that observed for native DmCaM (compare Fig. 3(C),(D) and 2(B)). When excess Eu^{3+} is present, detection of the Eu^{3+}_{aq} ion peak is hindered by an inherently broad band at ~ 579.1 nm for both mutants; therefore, it is likely that this band comprises both protein-bound and free Eu^{3+}_{aq}.

3.2. Time-resolved studies of wild type and mutant DmCaM

For cases where the $^7F_0 \rightarrow {}^5D_0$ transition of Eu^{3+} is not resolvable into separate peaks for each Eu^{3+} environment, time-resolution techniques are useful for examining the individual binding sites based on their differing excited-state lifetimes in H_2O or D_2O solution. The time-course of luminescence decay for Eu^{3+} bound to sites I and II of DmCaM, B3K, and B4K is described by a single exponential in both H_2O ($\tau = 0.40$ ms) and D_2O ($\tau = 2.45$ ms) solution. Beyond the addition of 2 equiv of Eu^{3+}, the resolution of two additional lifetime values in both media, signals Eu^{3+} ion coordination to sites III and IV of DmCaM (H_2O $\tau = 0.51$, 0.26 ms, D_2O $\tau = 2.05$, 0.58 ms Table 2); for B3K and B4K the number of Eu^{3+} lifetimes present in the excited-state decay depends on the mutant and the medium (H_2O or D_2O).

For B3K and B4K in H_2O solution, Eu^{3+} binding to the sites in the modified domain is characterized by a short-lived ($\tau = 0.23$ ms) and a long-lived ($\tau =$ 0.6–0.8 ms B3K; $\tau = 0.73$ ms B4K) species. The long lifetime value resolved for B4K has an appreciable amplitude and is detected at slightly lower metal-to-protein ratios that the 0.23 ms species. This finding suggests that the long-lived entity corresponds to the site in the C-terminal lobe with a greater affinity for the Eu^{3+} ion. For B3K, the intensity at time zero for the long-lived entity is maximized with excitation in the 579.4–579.6 nm range; however, the amplitude achieved is approximately one-tenth that observed for the 0.40 and 0.23 ms components, which makes the exact excited-state lifetime value difficult to define. This difficulty is reflected in the relatively large error associated with the reported τ value (Table 2).

At higher Eu^{3+} concentrations, a single excited-

Table 2
Data for determination of the number of water molecules, q, coordinated to the Eu^{3+} ions bound to *Drosophila melanogaster* calmodulin and the lysine series of mutants

Mutant	sites	τ_{D_2O}(ms)	τ_{H_2O}(ms)	q †
Wild type	I and II	2.45 ± 0.03	0.40 ± 0.01	2.2 ± 0.5
	III or IV	2.05 ± 0.05	0.51 ± 0.02	1.5 ± 0.5
	III or IV	0.58 ± 0.08	0.26 ± 0.02	2.2 ± 0.5
B3K	I and II	2.45 ± 0.03	0.40 ± 0.01	2.2 ± 0.5
	(A)			
	III or IV	2.45 ± 0.03 [a]	0.23 ± 0.01	4.1 ± 0.5 [a,c]
		1.95 ± 0.05 [b]	0.7 ± 0.1	4.0 ± 0.5 [b]
	(B)			
	III or IV	2.05 ± 0.10 [c]	0.23 ± 0.01	1.0 ± 0.5 [a,c]
			0.7 ± 0.1	0.9 ± 0.5 [b]
B4K	I and II	2.45 ± 0.02	0.40 ± 0.01	2.2 ± 0.5
	III or IV	1.83 ± 0.05	0.23 ± 0.01	4.0 ± 0.5
			0.73 ± 0.03	0.9 ± 0.5
B1K	I-IV	0.55 ± 0.80 [d]	0.26 ± 0.02	2.1 ± 0.5 [d]
				3.6 ± 0.5 [c]
		2.20 ± 0.10 [a]	0.47 ± 0.02	0.3 ± 0.5 [d]
			(579.5 nm)	1.8 ± 0.5 [c]
		2.20 ± 0.10	0.45 ± 0.02	0.4 ± 0.5 [d]
			(579.3 nm)	1.9 ± 0.5 [c]
		2.20 ± 0.10	0.70 ± 0.10 *	1.0 ± 0.5
B2K	I-IV	0.60 ± 0.10 [f]	0.26 ± 0.02	2.3 ± 0.5 [f]
				3.6 ± 0.5 [g]
		2.20 ± 0.10 [g]	0.50 ± 0.03	0.4 ± 0.5 [f]
				1.6 ± 0.5 [g]
	I-IV	0.60 ± 0.10 [f]	0.26 ± 0.02	2.3 ± 0.5 [f]
	alternate			3.6 ± 0.5 [h]
		2.35 ± 0.05 [h]	0.45 ± 0.03	0.6 ± 0.5 [f]
				1.9 ± 0.5 [h]
				1.7 ± 0.5 [i]
		1.63 ± 0.10 [i]	0.80 ± 0.10	0.9 ± 0.5 [h]
				0.7 ± 0.5 [i]

† $q = 1.05\left(\tau_{H_2O}^{-1} - \tau_{D_2O}^{-1}\right)$

* This value is not detectable at 579.3 nm

† Reported errors represent deviations associated with determination of the excited-state lifetime values; however, the largest source of uncertainty stems from the empirical fit to the data used to determine Eq.(1) [26].

[a-i] Denote combinations of excited-state lifetime values for calculation of q.

state lifetime value (1.83 ms) identifies the Eu^{3+} ions bound to sites III and IV of B4K in D_2O; one or two values are possible for B3K. Because the resolved lifetime values and their respective amplitudes are quite similar, we analyzed the multi-exponential decays as follows. If the luminescence decay trace obtained after the addition of 2.5 equiv of Eu^{3+} is subtracted from the subsequent data, then the resultant exponential is best described by a single lifetime value of 2.05 ms. However, if the data at 2.5 equiv are not subtracted, then the amplitude of the 2.45 ms value increases until the addition of ~3 equiv of Eu^{3+}, with concomitant resolution of a second excited-state lifetime value of 1.95 ms. The fit quality is equally good for both approaches. The short lifetime value (0.58 ms) observed for the wild type protein is not detected for either of the carboxyl-terminal mutants, which suggests that lysine substitution at site III or IV rearranges the C-terminal domain such that the deexcitation pathway responsible for this unusually short value is no longer available.

Using the reciprocals of the excited-state lifetimes (ms^{-1}) in H_2O and D_2O to calculate the number of H_2O molecules in the first coordination sphere of the protein-bound Eu^{3+} ion [26], we determined that two H_2O molecules are coordinated to the Eu^{3+} ions bound to sites I, II, and either site III or IV (τ = 0.26 ms) of DmCaM, while the remaining site (τ = 0.51 ms) has 1.5 H_2O molecules (Table 2). It is likely that two H_2O molecules are present at all of the binding sites in light of the extreme similarity of the amino acid sequences [27] and the static structures [3,28] between DmCaM and the two other previously characterized CaM isotypes (bovines testes and octopus), and the preferred Eu^{3+} coordination numbers of eight or nine (six ligands are derived from the protein). To determine the number of H_2O molecules coordinated to the Eu^{3+} ions at sites III and IV of DmCaM, the pairs of lifetime values were matched based on the differences in the amplitudes of the component exponentials in the H_2O and D_2O experiments.

For both B3K and B4K, we calculate two H_2O molecules coordinated to the Eu^{3+} ions bound at sites I and II, in good agreement with the wild type protein. For the sites in the modified domain (III and IV), 1 and 4 H_2O molecules are calculated for the 0.7 and 0.23 ms sites, respectively, thus indicating that the Eu^{3+} ion environments giving rise to these values differ significantly from their unmodified counterparts. It is probable that the 0.23 ms site (four H_2O molecules) represents the mutated site which completes the first coordination sphere of the Eu^{3+} ion by replacing the carboxylate oxygen ligands of the bidentate glutamic acid with two additional H_2O

molecules. The partner site (0.7 ms), which has only one H_2O molecule, apparently gains a ligand from the protein as a result of the mutation at the other site.

As with the spectral studies, time resolution of the individual Eu^{3+} ion environments for B1K and B2K reveals a Eu^{3+}-binding behavior significantly altered from that of the wild type protein. Unlike Eu^{3+} bound to the latter, which displays a single excited-state decay from the start of the titration, multiple exponentials are present for B1K and B2K from the beginning. The similarity of the different excited-state lifetime values at the titration outset makes resolution of the multiexponential decays difficult; in fact, the data are consistent with different combinations of τ values. Listed in Table 2 are the τ-values most consistent with all of the luminescence data. A further detailed discussion of the τ-values and their wavelength dependencies in H_2O and D_2O is given in a thesis [16]. Owing to the ambiguities in resolving the luminescence decays into component exponentials for B1K and B2K, it is not possible to match the lifetime values based on their individual amplitudes in H_2O and D_2O solution; therefore, various combinations were considered in calculating the number of H_2O molecules bound to the Eu^{3+} ion. As shown in Table 2, both B1K and B2K have Eu^{3+} ions with four, two, one or zero bound H_2O molecules.

In attempting to assign the τ-values to the individual metal-binding sites, we arrived at two most probable interpretations. Given the similarity in the Eu^{3+} lifetimes resolved for B1K and B2K, the following applies to both mutants. The first interpretation assumes that the mutations in the amino terminus do not cause any changes in the Eu^{3+} ion environments in the carboxyl terminus (sites III and IV). In this model, we assign the 0.26 ms value and one component of the inseparable 0.45–0.50 ms decay to sites III and IV, leaving the additional unresolved component and the long-lived decay (τ = 0.70 ms B1K; τ = 0.80 ms B2K) attributable to Eu^{3+} binding to sites I and II. This site assignment implies that, (i) the nonmutated partner site has only one Eu^{3+}-bound H_2O molecule and uses an additional ligand from the protein in coordinating the metal ion, and (ii) the modified site replaces the glutamate oxygen atoms with two ligands from the protein since two Eu^{3+}-bound H_2O molecules are calculated from the lifetimes measured in H_2O and D_2O (Table 2). In the second interpretation, the mutations in the N-terminus change one of the sites in the C-terminus such that the 0.45–0.50 ms value represents Eu^{3+} binding to both sites III and IV, and the remaining lifetime values are attributed to the mutated site (0.26 ms) and its partner (0.70 ms). In this case, the Eu^{3+} ion at the mutated site coordinates four H_2O molecules, the nonmutated site has one, and sites III and IV have zero, one, or two coordinated H_2O molecules. The second interpretation is preferred based on the observation that the amplitudes of the 0.55 ms (B1K) and 0.60 ms (B2K) lifetimes measured in D_2O are much smaller than those detected for the 0.26 ms species in H_2O, thereby suggesting that the Eu^{3+} ion environments represented by these lifetime values in H_2O and D_2O are not the same.

3.3. Intermetal ion distance measurements from Förster-type non-radiative energy transfer

In our earlier studies of BcaM [12] and OcaM [14], Förster-type non-radiative energy transfer [29] between excited Eu^{3+} ions and nearby Nd^{3+} ions bound at the four metal sites of the protein was exploited in measuring site—site distances that were in excellent agreement with the X-ray crystal structure of mammalian CaM. The same protocol outlined previously [12,14], is applied here to DmCaM, B3K, and B4K. The parameters and equations employed in the calculation, as well as the Eu^{3+} lifetimes in the absence (τ_o) and presence (τ_{Nd}) of energy transfer are given in Table 3. The distances obtained for sites I and II of DmCaM, B3K, and B4K (12.0 $\pm$ 0.5 Å) and sites III amd IV of DmCaM (11.1 $\pm$ 0.8 Å) and B4K (10.9 $\pm$ 0.8 Å) agree well with those measured from the X-ray crystal structure (12.4 and 10.9 Å for the N- and C-terminal sites, respectively; [28]). Owing to the low relative intensity of the 0.58 ms value that is observed for site III or IV in the absence of energy transfer, it was not possible to resolve a reduced lifetime value corresponding to this value for DmCaM in the analysis of the shortened excited-state decays. The separation of sites III and IV in B3K was not measured because of the ambiguity in the D_2O excited-state lifetime values for the carboxyl terminus; however, a shortened Eu^{3+} life-

Table 3
Parameters for Förster-type energy-transfer distance measurements between the metal-binding sites of *Drosophila melanogaster* calmodulin and the carboxyl-terminal mutants

Mutant	sites	τ_0(ms)	τ_{Nd}(ms)	E [a]	ϕ [b]	R_0(Å) [b,c]	r(Å) [d,e]
Wild type	I & II	2.42 ± 0.02	1.52 ± 0.02	0.372	0.70	11.0	12.0 ± 0.5
	III & IV	2.06 ± 0.04	1.33 ± 0.04	0.354	0.39	10.0	11.1 ± 0.8
B3K	I & II	2.44 ± 0.03	1.53 ± 0.03	0.373	0.70	11.0	12.0 ± 0.5
B4K	I & II	2.43 ± 0.03	1.53 ± 0.05	0.370	0.70	11.0	12.0 ± 0.5
	III & IV	1.83 ± 0.05	1.15 ± 0.05	0.372	0.39	10.0	10.9 ± 0.8

[a] $E = 1 - (\tau_{Nd}/\tau_o)$.
[b] Ref. [12].
[c] $R_{0^6} = (8.78 \times 10^{-25})\kappa^2\phi\eta^{-4}J$; $J = 1.4 \times 10^{-17}$ cm^6 mol^{-1}
[d] $r = R_0[(1 - E)/E]^{1/6}$.
[e] The principal uncertainty in the distance measurements arises from estimates of the quantum yield of the protein-bound Eu^{3+} ions, Ref. [12].

time is detected in the presence of Nd^{3+}, and is indicative of metal ion binding to both sites in this domain (sites III and IV).

3.4. Steady state experiments and dissociation constant measurements for wild type and mutant DmCaM

For steady state experiments where the emission intensity is collected at a single excitation wavelength, the observed luminescence intensity is proportional to the concentration of Eu^{3+} species contributing at that wavelength. As shown by the titration experiment for DmCaM (15 μM) in Fig. 4, the straight line portion of the curve indicates that two Eu^{3+} ions bind quantitatively to the protein, followed by weaker binding to the lower affinity site(s). It should be noted that the slope of the straight line portion of the titration curve, and the magnitude of the 'burst' after the addition of 2–3 equiv of Eu^{3+}, reflect the differences in the luminescence intensity among the several sites of protein-bound Eu^{3+} ions upon excitation with 579.35 nm light.

Dissociation constants for two of the four binding events are calculated from titration curves obtained upon excitation with laser light pulsed at 579.35 (Fig. 4) and 579.50 nm (data not shown). Data obtained at both excitation wavelengths is necessary to determine the dissociation constant for both of the lower affinity sites. In calculating the theoretical fit to the data, Eu^{3+} ion, protein, and complex concentrations (in this case steady state luminescence intensity) are input into the program EQUIL, along with a set of equilibrium binding equations (i.e. the binding model; one equation per class of site), estimates of the individual amplitudes based on resolution of the component bands in the excitation spectra, and initial guesses for the dissociation constants. Poor initial guesses can cause convergence at a local minimum; therefore, knowledge of the system under study is helpful in formulating these initial values. Further, the robustness of a given fit to the data can be tested by supplying different starting values (K_ds) and by

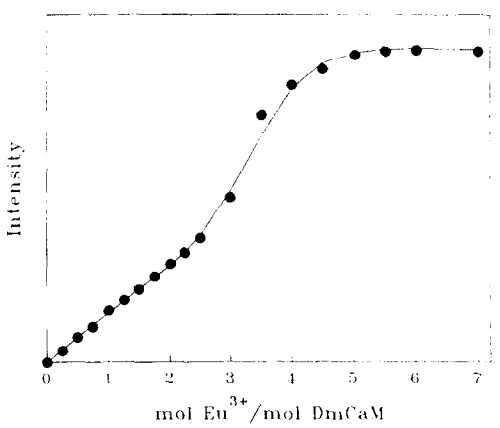

Fig. 4. Intensity of the $^7F_0 \rightarrow {}^5D_0$ ($\lambda_{ex} = 579.35$ nm) excitation band as afunction of total equivalents of Eu^{3+} added to apo-DmCaM (15 μM). The solid line represents the theoretical fit of the data with dissociation constants $K_{1,2} = 0.01$ μM, $K_3 = 0.40$ μM, and $K_4 = 1.8$ μM. Non-time-resolvedtitration data obtained at various excitation wavelengths was analyzed simultaneously in arriving at the reported K_d values.

evaluating different binding models. Mathematical formulations and model acceptance criteria have been presented elsewhere [22].

The protein concentrations employed in the DmCaM experiments are 3 orders of magnitude larger than the dissociation constant for Eu^{3+} in the two tight sites, and therefore, this value was not determined by this experiment. Given the similarity between DmCaM and the CaM isotypes characterized previously, the average K_d value calculated for Eu^{3+} binding to sites I and II of BCaM and OCaM (~ 0.01 μM; [14]), was held constant in the analysis of the DmCaM titration data. Using a competitive binding model in which the two tight sites are treated as one class of site, and assuming two independent binding events for sites III and IV, dissociation constants of 0.40 and 1.8 μM are calculated for the titration curves (Fig. 4 and Table 4). The dissociation constants derived for Eu^{3+} binding are site or intrinsic constants, in contrast to the Ca^{2+}-binding experiments [5], which measured macroscopic dissociation constants. The titration data were also analyzed using a two-class model comprised of two high-affinity sites ($K_d \approx 0.01$ μM), and two independent, equivalent low-affinity sites, which yielded a dissociation constant of 1.1 μM. This model produced an inferior fit to the data (not shown).

The best theoretical fit to the titration curves for B3K and B4K is obtained with a competitive binding model that comprises four Eu^{3+} ions bound in three independent classes of site. As shown in Fig. 5(A), 5(B) and Fig. 6, one class contains two high-affinity sites ($K_d \approx 0.01$ μM); an initial guess for these two tight sites was made based on the results for the native protein. The quantitative binding behavior of the first two Eu^{3+} ions added to B3K (Fig. 5(A)) or B4K (Fig. 5(B)) and the nearly identical luminescence properties observed for the tight Ln^{3+}-binding sites (I and II) in these mutants and wild type DmCaM justify this assumption. The remaining two classes in the model are comprised of lower affinity sites having best fit K_d-values of 1.5 and 2.5 μM for B3K, and 3.5 and 13 μM for B4K (Table 4). A combination of data from steady state (λ_{ex} =

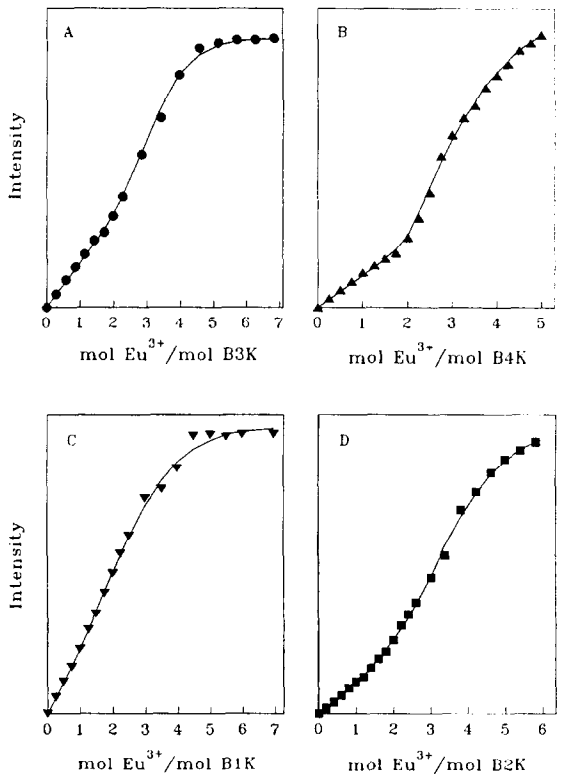

Fig. 5. Intensity of the $^7F_0 \rightarrow {}^5D_0$ excitation band as a function of total equivalents of Eu^{3+} added to (A) B3K (λ_{ex} = 579.35 nm; 13 μM), (B) B4K (λ_{ex} = 579.50 nm; 10 μM), (C) B1K (λ_{ex} = 579.35 nm; 15 μM), and (D) B2K (λ_{ex} = 579.50 nm; 15 μM). The solid line, in each case, represents the theoretical fit using the dissociation constants reported in Table 4.

Table 4
Calculated dissociation constants (μM) for Eu^{3+} ion binding to *Drosophila melanogaster* calmodulin and the lysine series of mutants

Mutant	K_1	K_2	K_3	K_4
Wild type	0.01 [a]	0.01	0.40 ± 0.10	1.8 ± 1.0
B3K	0.01 [a]	0.01	1.5 ± 0.5	2.5 ± 0.6
B4K	0.01 [a]	0.01	3.5 ± 1.0	13 ± 5
B1K	0.04 ± 0.02	1.5 ± 0.4	3.5 ± 0.1	9.1 ± 1.5
B2K	0.04 ± 0.02	0.69 ± 0.10	1.2 ± 0.1	12 ± 4

In arriving at the appropriate model to describe Eu^{3+} binding to each protein, the binding isotherms were fit with various models that evaluated the total number of protein-bound Eu^{3+} ions (3 or 4), the number of classes of binding site (2, 3, or 4) and the number of Eu^{3+} environments present in each class. Minimization of χ^2 and visual inspection of the agreement between the theoretical fit and the titration curve provided the basis for accepting or rejecting a particular binding model.

[a] Value estimated from the dissociation constant determined for sites I and II of bovine and octopus calmodulin, Ref. [14].

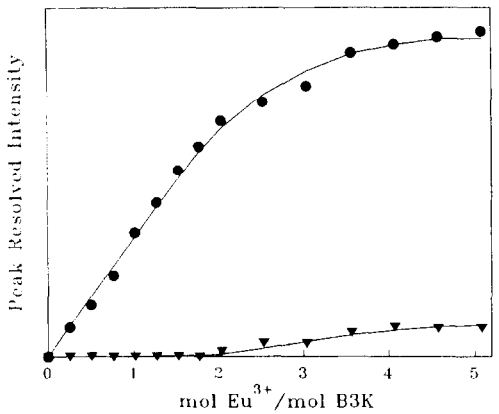

Fig. 6. Curve-resolved $^7F_0 \rightarrow {}^5D_0$ excitation spectrum peak intensities plotted as a function of Eu^{3+} added to B3K (13 μM). The solid line represents the theoretical fit to the data for the (●) 579.24, 579.38 nm peaks combined ($K_{1,2} = 0.01$ μM, $K_4 = 2.5$ μM), and the (▼) 579.63 nm peak ($K_3 = 1.5$ μM).

579.35 nm, Fig. 5(A); $\lambda_{ex} = 579.55$ nm, data not shown), time-resolved ($\lambda_{ex} = 579.55$ nm, data not shown), and peak-resolved spectral titrations (Fig. 6) was analyzed simultaneously to calculate the dissociation constants for B3K, while steady state titration data ($\lambda_{ex} = 579.28$, 579.30, 579.50 nm) was employed for B4K (Fig. 5(B)).

Of all the mutants studied, the Eu^{3+}-binding affinity of all of the sites in the protein molecule is least affected by mutation of site III (B3K), a finding which concurs with the lack of perturbations in the Eu^{3+} spectral data relative to WT-DmCaM, and is similar to the results of Ca^{2+}-binding studies previously conducted for this series of mutants [5]. Assignment of the measured dissociation constants to either site III or IV is ambiguous because the mutated site still binds the Eu^{3+} ion. The possible site assignments have been outlined previously [16]; however, only the preferred interpretation is presented here. In this model, it is assumed that the largest dissociation constant represents Eu^{3+} binding to site III, in accordance with the Ca^{2+}-binding studies of B3K and B4K [5,30], which demonstrated that binding at the mutated site is effectively eliminated for the range of Ca^{2+} concentrations at which CaM functions. For native DmCaM, if the tighter site in the pair ($K_d = 0.4$ μM) is site III, then the Glu104 → Lys substitution decreases the Eu^{3+}-binding affinity by a factor of 6 ($K_d = 2.5$ μM B3K), and has no effect on site IV ($K_d = 1.5$ μM B3K, 1.8 μM DmCaM). This assignment is consistent with the interpretation of the excited-state lifetime data offered above in which the nonmutated partner site (IV) gains a ligand, and consequently produces tighter Eu^{3+} ion binding at that site. Following the interpretation of the binding data presented for B3K, site IV has a 1.8 μM dissociation constant in the native protein which is increased by a factor of about 10–13 μM (the largest K_d value) in B4K, while the binding affinity of the partner site (III) is reduced by the same amount (K_d 0.4 → 3.5 μM). These results reveal that mutation of site IV has a greater effect on the metal ion binding affinity of its partner site in the domain than does mutation of site III.

For both amino terminal mutants, the binding model which best describes all of the titration data consists of four independent binding sites. For B1K, simultaneous analysis of steady state ($\lambda_{ex} = 579.35$, 579.55 nm), and time-resolved ($\lambda_{ex} = 579.50$ nm) titration data was conducted, while determination of the dissociation constants for B2K incorporated steady state ($\lambda_{ex} = 579.35$, 579.50 nm), and time-resolved ($\lambda_{ex} = 579.35$ nm) titration data into the analysis. A single tight site with a calculated dissociation constant of ~ 0.04 μM is present for B1K and B2K. The protein concentration employed in the experiments does not allow for accurate determination of this tight site; however, a K_d value of 0.04 μM significantly reduced χ^2 as compared to 0.01 μM. The larger value is reported here indicates that binding at the high affinity pair of sites is reduced in these mutants relative to the wild type protein and the carboxyl-terminal mutants. The lower affinity sites of B1K have dissociation constants of 1.5, 3.5, and 9.1 μM (Fig. 5(C), Fig. 7), while the results for B2K are similar with dissociation constants of 0.69, 1.2, and 12 μM (Fig. 5(D)).

The time-resolved binding isotherm for B1K (Fig. 7) is helpful in revealing the impact of the mutations on the Eu^{3+} ion affinity of all of the sites. The following interpretation applies to both B1K and B2K. Recalling the second binding-site distribution of the Eu^{3+} lifetimes outlined above, the two weakest sites are I and II ($\tau = 0.70$ ms, $K_d = 3.5$ μM; $\tau = 0.26$ ms, $K_d = 9.1$ μM — see Fig. 7), and either site III or IV increases its Eu^{3+} ion affinity ($\tau = 0.47$ ms, $K_d = 0.04$ μM). The Eu^{3+} binding affinity

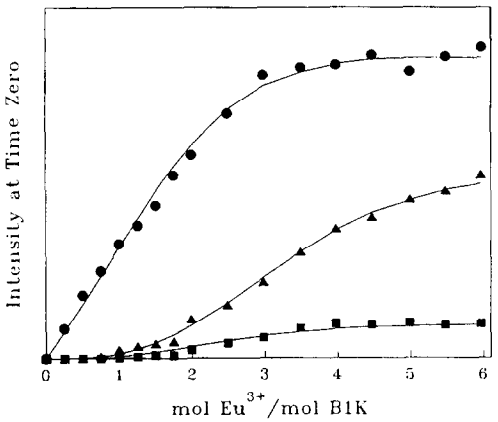

Fig. 7. Intensities at time zero for the exponential decay of the $^7F_0 \rightarrow {}^5D_0$ transition (λ_{ex} = 579.50 nm) of the Eu^{3+} ion bound to B1K (15 μM) plotted as a function of total equivalents of Eu^{3+} added. The solid lines represent the theoretical fit of the data with the dissociation constants indicated: (●, τ = 0.47 ms) K_1 = 0.04 μM, K_2 = 1.5 μM; (▲, τ = 0.26 ms) K_4 = 9.1 μM; and (■, τ = 0.70 ms) K_3 = 3.5 μM.

of the remaining site in the C-terminus (τ = 0.47 ms, K_d = 1.5 μM) is either the same as or slightly weaker than the corresponding site in the wild type protein. Although this site assignment involves both an alteration in the Eu^{3+} ion environments, and a redistribution of the high- and low-affinity sites in the protein, it predicts that the mutated site has the weakest Eu^{3+}-binding affinity, in accord with the results of Ca^{2+}-binding studies [5]. This assignment also suggests structural consequences that are similar to those proposed for the carboxyl-terminal mutants.

4. Discussion

4.1. Eu^{3+} binding to wild type DmCaM

It is clear from Eu^{3+} spectroscopy that the Eu^{3+}-binding properties of *Drosophila* CaM are nearly identical to those of the previously characterized vertebrate (bovine testes; [12,13]) and invertebrate (octopus; [14]) CaM. For native DmCaM (and the mutant proteins), the present data are consistent with a simple Eu^{3+} ion binding scheme involving independent, noninteracting sites. Given the cooperative behavior observed for Ca^{2+} binding to the high-affinity sites (III and IV) of the wild type protein [5,30], it is quite possible that Eu^{3+} ion coordination to sites I and II (high-affinity Ln^{3+}-binding sites) involves cooperativity as well. Studies designed to evaluate the cooperativity of Eu^{3+} binding to CaM are currently underway in our laboratory.

4.2. Eu^{3+} binding to the carboxyl-terminal mutants of DmCaM

Site-directed mutagenesis of the individual metal-binding sites of DmCaM allows for selective interrogation of the role of each site in the structure and function of the protein, as well as for the evaluation of the importance of a single amino acid residue to the metal ion binding ability of an individual loop. For mutation of either of the low-affinity Ln^{3+}-binding sites (III or IV), the spectroscopic data reveal that the high-affinity sites (I and II) of the resultant protein remain intact. For example, in H_2O or D_2O solution the Eu^{3+} excited-state lifetime values measured for the Eu^{3+} ion bound to sites I and II of either B3K or B4K match the values obtained for the same sites in the wild type protein (Table 2). The excitation spectra recorded for the Eu^{3+} ion bound to sites I and II of B3K are indistinguishable from native DmCaM, while for B4K the spectra reveal some minor differences. However, given the identical site-site distances for DmCaM and the carboxyl-terminal mutants measured via Förster energy transfer, and the agreement of these distances with the X-ray crystal structure [28], the structural modifications within the domain are minimal. Furthermore, CD studies of B3K and B4K [6], and NMR studies of B3Q and B4Q [33] in the presence and absence of Ca^{2+} indicate that the folded structure of the N-terminal domain is not significantly altered by the mutations. The NMR studies also show that the amino acid markers used to follow Ca^{2+} binding at sites I and II behave like the wild type protein.

In prior ^1H NMR studies of Ca^{2+} binding [31] it was found that although the Ca^{2+} ion is bound weakly by the modified site I, the chemical shift observed for Thr26 (loop I) suggests that deformation of the metal binding site is caused by an altered Ca^{2+} conformation at the mutated site, or an altered coordination environment at site I when the partner site (II) is mutated. In the present study, the excited-

state lifetime data for the Eu^{3+} ion bound to sites III and IV provide additional insight into the impact of the mutations on Eu^{3+} ion coordination to the modified site and its partner. It is apparent from the number of H_2O molecules calculated from the excited-state lifetime values in H_2O and D_2O that the mutated site compensates for the loss of the bidentate glutamic acid residue by coordinating two additional H_2O molecules. This appears to have consequences for the partner site which has only one H_2O molecule bound to the Eu^{3+} ion and, by inference, adds another ligand from the protein. Molecular modelling studies of the metal-binding sites in the mutant proteins have shown that it is possible for one of the other carboxylate moieties in the binding loop to coordinate the metal ion in a bidentate fashion. Based on the X-ray crystal structure of DmCaM [28], the $O_{\delta 2}$ atoms of Asp 95 (site III) and Asp133 (site IV) which are positioned 3.6 and 3.2 Å away from the Ca^{2+} ion, respectively, are potential ligands for the Eu^{3+} ion, and could coordinate with a relatively minor conformational change. The altered Ca^{2+}-bound conformation detected for the C-terminal domain using far- and near-UV CD[5] and ^1H NMR [31], suggests that reorganization of the ligands in at least one of the sites is likely.

The results of the steady state titrations indicate quantitative binding behavior for the first two Eu^{3+} ions added to B3K and B4K (Fig. 5(A), 5(B)), and calculation of the corresponding dissociation constants establishes that mutation of sites III or IV has little to no effect on the Eu^{3+} ion affinity of the sites in the N-terminus (I and II). However, it should be noted that given the protein concentrations employed in the experiments, a decrease in the Eu^{3+} ion affinity of sites I and II would only be detected if the new dissociation constant were at least an order of magnitude larger than the old one. With regard to Eu^{3+} binding in the modified domain, the finding that modification of loop IV is more damaging than mutation of loop III is consistent with the results of Ca^{2+}-binding studies and the evaluation of the structural consequences of the mutations by electrophoresis [5]. Compared with the wild type, B4K displays the most pronounced difference in electrophoretic mobility in both the presence and absence of Ca^{2+}. In addition, the change in the intensity of CD signals at 222 and 280 nm indicate that the lysine substitution at site IV is more detrimental to Ca^{2+}-induced conformational changes than the corresponding change in site III [6]. In these same studies, B3K displays the expected electrophoretic mobility, eventually attains a conformation in which the environment of Tyr138 resembles that of the native protein, and exhibits CD signals that are in the similar to those of the wild type.

4.3. Eu^{3+} binding to the amino-terminal mutants of DmCaM

The luminescence data obtained for the amino-terminal mutants confirm that modification of either site I or II alters the Eu^{3+}-binding behavior and the metal-bound conformation of the domain. For both B1K and B2K, the presence of three bands in the $^7F_0 \rightarrow {}^5D_0$ excitation spectrum at the titration outset suggests that as many as three sites are competing initially for the Eu^{3+} ion. In general, two of the three peaks resolved fall at peak positions observed for the wild type protein, while the excitation maximum of the third band is quite variable and shifted to lower wavelengths relative to the other bands. It is tempting to speculate that this blue-shifted peak represents Eu^{3+} bound to the mutated site; however, its early appearance in the excitation spectrum would imply that the modified site is not the weakest. Alternatively, the excitation band at ~ 579.1–579.2 nm may represent an altered Eu^{3+} environment for one of the other sites. In this case, the partner site is a likely candidate, as NMR studies of B1Q and B2Q [31] have identified altered Ca^{2+}-bound conformations for sites I and II in both mutants. Comparison of the excitation peak widths (fwhm) provides additional information about the resultant Eu^{3+} environments. Only the peak at ~ 579.6 nm maintains a peakwidth similar to a band observed for native DmCaM; in general, the other bands are significantly broader. Rigid metal-binding sites generally exhibit narrow excitation bands. For example, the single excitation band observed for Eu^{3+} bound to the fivefold channel site of satellite tobacco necrosis virus has a fwhm of 0.21 nm (6.5 cm^{-1}; [32]) compared with 0.32–0.68 nm (10–20 cm^{-1}) for other Ca^{2+}-binding proteins [23,33]. The relative breadth of the bands observed for the

amino-terminal mutants suggests that the resulting metal-binding sites are less rigid than the corresponding sites in the wild type protein or carboxyl-terminal mutants. However, a fourth unresolved band with an excitation maximum in between the bands at 579.1 and 579.4 nm could shift the derived peak positions and result in apparent band broadening as well.

As with the C-terminal mutants, the preferred interpretation of the excited-state lifetime data indicates that the mutated site coordinates two additional H_2O molecules in compensating for the loss of the bidentate glutamic acid residue, and the partner site gains a ligand from the protein, thereby displacing an H_2O molecule. In the X-ray crystal structure of DmCaM [28], the $O_{\delta 2}$ atoms of Asp20 and Asp24 in site I, which are positioned 3.8 Å away from the metal ion, and the $O_{\delta 2}$ atom of Asp56 in site II (4.0 Å), are the leading candidates for additional ligation. In the case of B1K and B2K, it appears that the structural consequences of mutation extend to the metal-binding sites in the carboxyl-terminal lobe, where a change in the Eu^{3+} coordination environment is also observed for at least one of the sites in the distal domain. CD studies [5,6] of the N-terminal mutants in the absence of Ca^{2+} have shown an altered conformation for Tyr138 (loop IV), which suggests that the structure of the C-terminus is influenced by the mutations in the opposite domain, and that a global conformational change takes place.

The results of the luminescence experiments establish that a high-affinity pair of sites no longer exists for either B1K or B2K, rather, the data suggest that the Eu^{3+}-binding behavior has been altered for all of the metal ion binding sites in the protein molecule. The proposed binding model and resultant dissociation constants reveal a single high-affinity site, though it is unclear whether or not this is the nonmutated partner site. The impact of mutation of either site I or II on Eu^{3+}-binding behavior is best compared to the Ca^{2+}-binding properties of the C-terminal mutants, because this domain contains the high-affinity Ca^{2+}-binding sites. The results of Ca^{2+}-binding studies of B3K and B4K [5] imply that three noninteracting binding events occur for the site III and IV mutants, in addition to NMR studies of the glutamine mutants (B3Q, B4Q; [31]) that suggest that sites I and II may bind Ca^{2+} before the nonmutated partner site. Further, although the NMR studies do not reveal an increase in the Ca^{2+}-binding affinity of sites I and II (the low-affinity Ca^{2+}-binding pair) as a result of the mutations, stopped-flow experiments [34] indicate that the dissociation rate of the Ca^{2+} ion from these sites is reduced relative to the native protein. Therefore, it is reasonable to propose that substantial reorganization of the ligating residues and concomitant redistribution of the Eu^{3+}-binding affinities occurs. By destroying the high-affinity pair of Ln^{3+}-binding sites in the N-terminus, it is possible that a more Ca^{2+}-like binding behavior results, thereby causing a tightening of the C-terminal sites.

5. Conclusion

The present study illustrates the sensitivity of laser-excited Eu^{3+} luminescence to the fine details of Eu^{3+} binding to a native CaM isotype relative to a series mutants, in which the invariant glutamic acid residue in position 12 of each binding loop is replaced by a lysine residue. The results of the Eu^{3+} luminescence studies demonstrate clearly that the modified site coordinates a Eu^{3+} ion, albeit with diminished affinity. The detection of a Eu^{3+} ion environment with four coordinated H_2O molecules, in contrast to the two H_2O molecules typically observed for Eu^{3+} ions bound to calmodulin, supports the assertion that the Eu^{3+} ion binds to the weakened, mutated site. The observation of energy transfer between Eu^{3+} and Nd^{3+} ions bound to sites III and IV of B3K and B4K provides further proof that Eu^{3+} binds to the modified site.

The results of the Eu^{3+} luminescence studies demonstrate that a change in the metal-binding environment does not affect the Ca^{2+}- and Eu^{3+}-binding behavior in the same manner. It is unclear why the Ca^{2+}-binding ability of the lysine series of mutants is impaired much more than the Eu^{3+}-binding ability; however, it should be noted that Ln^{3+} ions are invariably bound more tightly than Ca^{2+} ions for a given system, and from system to system the difference in dissociation constants between Ca^{2+} and Ln^{3+} range over several orders of magnitude [7]. The reorganization process that fosters Eu^{3+} ion coordination appears to be analogous for each modified site, given the nearly identical excited-state life-

time values measured for all of the mutants. These findings suggest a flexibility in the binding loops that is revealed by the Eu^{3+} luminescence studies.

The ability of the mutated site to coordinate Eu^{3+} much more strongly than Ca^{2+}, contrasts the binding behavior of these two ions; however, a closer examination of the results reveals similar trends for Eu^{3+} and Ca^{2+} ligation. For example, mutation of either of the low-affinity sites (III or IV, Eu^{3+}; I or II, Ca^{2+}) produces minor changes in the binding affinity of the tight pair of sites and the metal-bound conformation of the opposite lobe. Conversely, mutation of either of the high-affinity sites (I or II, Eu^{3+}; III or IV, Ca^{2+}) destroys the quantitative binding behavior of the pair, and allows the remaining sites to compete independently for the metal ion. This finding suggests that regardless of which pair of sites in the protein exhibit high affinity for a particular metal ion, the binding behavior of the entire protein molecule is governed by initial binding of metal ions to the tight pair of sites. In addition, the Eu^{3+} luminescence, Ca^{2+} -binding, and structural studies, demonstrate that for their respective domains, mutation of site II or IV produces a larger impact than modification of site I or III. Further, with regard to the overall impact on metal-binding affinity, the mutation of site III (B3K) causes the smallest reductions in affinity for Eu^{3+}, an observation that nicely parallels results of enzyme activation studies which showed that mutation of site I has the mildest effect on Ca^{2+} binding and Ca^{2+}-induced conformational change [35]. These observations are consistent with the structural similarities of loops II and IV, and loops I and III, which appear to arise from the high homology of their flanking helices [1], and points to the fact that site II or IV is the dominant site for a given domain, regardless of the metal ion (Ca^{2+} or Eu^{3+}) coordinated to the sites.

Acknowledgements

The National Science Foundation provided funds for the purchase of the laser system (Grant CHE-9123801 to W.D.H.) The authors wish to thank Dr. Sarah Burroughs Teneza and Dr. Steven T. Frey for many hours of helpful discussion.

References

[1] N.C.J. Strynadka and M.N.G. James, Annu. Rev. Biochem., 58 (1989) 951–998.
[2] B.J. Marsden, G.B. Shaw and B.D. Sykes, Biochem. Cell. Biol., 68 (1990) 587–601.
[3] Y.S. Babu, C.E. Bugg and W.J. Cook, J. Mol. Biol., 254, (1988) 191–204.
[4] K. Beckingham, J. Biol. Chem., 266, (1991) 6027–6030.
[5] J.F. Maune, C.B. Klee and K. Beckingham, J. Biol. Chem., 267, (1992) 5286–5295.
[6] J.F. Maune, K. Beckingham, S.R. Martin and P.M. Bayley, Biochemistry, 31 (1992) 7779–7786.
[7] W.DeW. Horrocks, Jr., in G.L. Eichhorn and L.G. Marzilli (Eds.), Advances in Inorganic Biochemistry, Elsevier, New York, 1982, pp. 201–262.
[8] W.DeW. Horrocks, Jr., Methods Enzymol., 226 (1993) 495–538.
[9] S.R. Martin, A. Tellemann Andersson, P.M. Bayley, T. Drakenberg and S. Forsén, Eur. J. Biochem., 151 (1985) 543–550.
[10] C.-L.A. Wang, P.C. Leavis and J. Gergely, Biochemistry, 23 (1984) 6410–6415.
[11] A. Andersson, S. Forsén, E. Thulin and H.J. Vogel, Biochemistry, 22 (1983) 2039–2313.
[12] W.DeW. Horrocks, Jr. and J.M. Tingey, Biochemistry, 27 (1988) 413–419.
[13] P. Mulqueen, J.M. Tingey and W.DeW. Horrocks, Jr., Biochemistry, 24 (1985) 6639–6645.
[14] J. Bruno, W.DeW. Horrocks, Jr. and R.J. Zauhar, Biochemistry, 31 (1992) 7016–7026.
[15] J.S. Fritz, R.T. Oliver and D.J. Pietrzyk, Anal. Chem., 30 (1958) 1111–1114.
[16] J. Bruno (1993) Ph.D. Thesis, The Pennsylvania State University, University Park, PA.
[17] S.T. Frey (1994) Ph.D. Thesis, The Pennsylvania State University, University Park, PA.
[18] J.M. Tingey (1987) Ph.D. Thesis, The Pennsylvania State University, University Park, PA.
[19] D.W. Marquardt, J. Soc. Ind. Appl. Math., 11 (1963) 431–441.
[20] C.W. McNemar and W. DeW. Horrocks, Jr., Appl. Spectrosc., 443 (1989) 816–821.
[21] C.W. McNemar (1988) Ph.D. Thesis, The Pennsylvania State University, University Park, PA.
[22] R.F. Goldstein and E. Leung, Anal. Biochem., 190 (1990) 220–232.
[23] C.W. McNemar and W. DeW. Horrocks, Jr., Biochim. Biophys. Acta. 1040 (1990) 229–236.
[24] M.T. Henzl, W.D. McCubbin, C.M. Kay and E.R. Birnbaum, J. Biol. Chem., 260 (1985) 8447–8455.
[25] S.E. Burroughs and W. DeW. Horrocks, Jr., Biochemistry, 33 (1994) 10428–10436.
[26] W. DeW. Horrocks, Jr. and D.R. Sudnick, Acc. Chem. Res., 14 (1981) 384–392.
[27] V.L. Smith, K.E. Doyle, J.F. Maune, R.P. Munjaal and K. Beckingham, J. Mol. Biol., 196 (1987) 471–485.

[28] D.A. Taylor, J.S. Sack, J.F. Maune, K. Beckingham and F.A. Quiocho, J. Biol. Chem., 266 (1991) 21375–21380.
[29] T. Förster, Ann. Phys. Leipzig, 2 (1948) 55–75.
[30] J.F. Maune, (1991) Ph.D. Thesis, Rice University, Houston, TX.
[31] M.A. Starovasnik, D.-R. Su, K. Beckingham and R.E. Klevit, Protein Sci., 1 (1992) 245–253.
[32] S.E. Burroughs, G. Eisenman and W. De W. Horrocks, Jr. Biophys. Chem., 42 (1992) 249–256.
[33] A.P. Snyder, D.R. Sudnick, V.K. Arkle and W. DeW. Horrocks, Jr. Biochemistry, 20 (1981) 3334–3339.
[34] S.R. Martin, J.F. Maune, K. Beckingham and P.M. Bayley, Eur. J. Biochem., 205 (1992) 1107–1114.
[35] Z.H. Gao, J. Krebs, M.F.A. VanBerkum, M.-J. Tang, J.F. Maune, A.R. Means and K. Beckingham, J. Biol. Chem., 268 (1993) 20096–20104.